World Academy of Science, Engineering and Technology
International Journal of Mechanical and Mechatronics Engineering
Vol:4, No:10, 2010

Atomic Force Microscopy (AFM) Topographical Surface Characterization of Multilayer-Coated and Uncoated Carbide Inserts

Samy E. Oraby and Ayman M. Alaskari

***Abstract*—**In recent years, scanning probe atomic force microscopy SPM AFM has gained acceptance over a wide spectrum of research and science applications. Most fields focuses on physical, chemical, biological while less attention is devoted to manufacturing and machining aspects. The purpose of the current study is to assess the possible implementation of the SPM AFM features and its NanoScope software in general machining applications with special attention to the tribological aspects of cutting tool. The surface morphology of coated and uncoated as-received carbide inserts is examined, analyzed, and characterized through the determination of the appropriate scanning setting, the suitable data type imaging techniques and the most representative data analysis parameters using the MultiMode SPM AFM in contact mode. The NanoScope operating software is used to capture realtime three data types images: "*Height*", "*Deflection*" and "*Friction*". Three scan sizes are independently performed: 2, 6, and 12 μm with a 2.5 μm vertical range (Z). Offline mode analysis includes the determination of three functional topographical parameters: surface "*Roughness*", power spectral density "*PSD*" and "*Section*". The 12 μm scan size in association with "*Height"* imaging is found efficient to capture every tiny features and tribological aspects of the examined surface. Also, "*Friction*" analysis is found to produce a comprehensive explanation about the lateral characteristics of the scanned surface. Configuration of many surface defects and drawbacks has been precisely detected and analyzed.

***Keywords*—**SPM AFM contact mode, carbide inserts, scan size, surface defects, surface roughness, PSD.

I. Introduction

SINCE its invention in 1986 by Binnig, Quate, and Gerber [1] the atomic force microscope AFM has become an indispensable tool for investigators in various applications; physical [2], [3], chemical [4]-[6], tribologyical and mechanical materials properties [7], [21], biological [22]-[26] and, biomechanical and electromechanical [27], [28]. Today, extensive imaging modalities have been implemented on the AFM under the umbrella of scanning probe microscopy SPM [22], [29]-[31]. In addition to topographical imaging, SPM has been used to measure magnetic fields, friction gradients, potentials, capacitance, current flow, piezo response, and temperature across a diverse array of samples [32].

AFM relies on a mechanical probe for generation of magnified images of surfaces down to nanometer resolution. It usually operates by scanning an ultra small tip (radius<10nm), supported on a 100-200 μm long force-sensing cantilever, over the sample and thereby producing a three-dimensional surface image of a spatial resolutions of a few nanometers and below. Probe-sample interactions induce bending and torsion of the cantilever typically measured through a laser deflection signal change that is recorded on a photodetector [33]-[38]. A feedback control system responds to those changes by adjusting the tip-sample distance in order to maintain a constant deflection/ distance to the sample surface. This vertical movement of the tip is translated into a topographical image of the surface with accuracy of few μm or less.

Generally, SPM techniques are classified, as described in Fig. 1, with specific features and operating setting assigned for a specific application. In most imaging modes there is a primary and a corresponding derivative mode. One of the useful derivative modes in contact mode is the lateral force microscopy LFM with major implementations in friction and tribology on the nanometer scale [7], [9]-[10], [13], [14], [19], [39]-[44]. Non imaging techniques are usually nano-indenting and nano-scratching with applications in mechanical and wear testing of materials [44]-[50].

II. Fundamentals and Hardwaere

The MultiMode SPM, Fig. 2, consists of seven major hardware components: SPM, controller, computer, keyboard, mouse, display monitor and control monitor. The MultiMode SPM AFM uses a microfabricated cantilever made of silicon or silicon nitride with a sharp tip that physically touches the surface of interest. The cantilever raster-scans the sample while its deflection or oscillation amplitude is measured. These measurements are performed with an optical tracking system that uses a segmented photodetector to track the reflection of a laser or superluminescent diode off the back of the cantilever. Detected changes in cantilever deflection or oscillation are corrected to a setpoint value by actuating the cantilever in Z via a feedback-controlled piezo. These correction voltages sent to the Z piezo are recorded and correlated to a voltage-distance calibration factor in order to determine the height at a given XY coordinate. More details

S. E. Oraby is with the College of Technological Studies, PAAET, B.O. Box 42325 Shuwaikh 70654, KUWAIT (corresponding author phone: +96599549019; fax: +96524832751; e-mail: se.oraby@ paaet.edu.kw).

A. M. Alaskari is with the College of Technological Studies, PAAET, B.O. Box 42325 Shuwaikh 70654, KUWAIT (phone: +96599655549; fax: +96524832751; e-mail: aalaskari@ gmail.com).

about system hardware and calibration procedures and as well as design and performance improvement aspects can be found in [51]-[59].

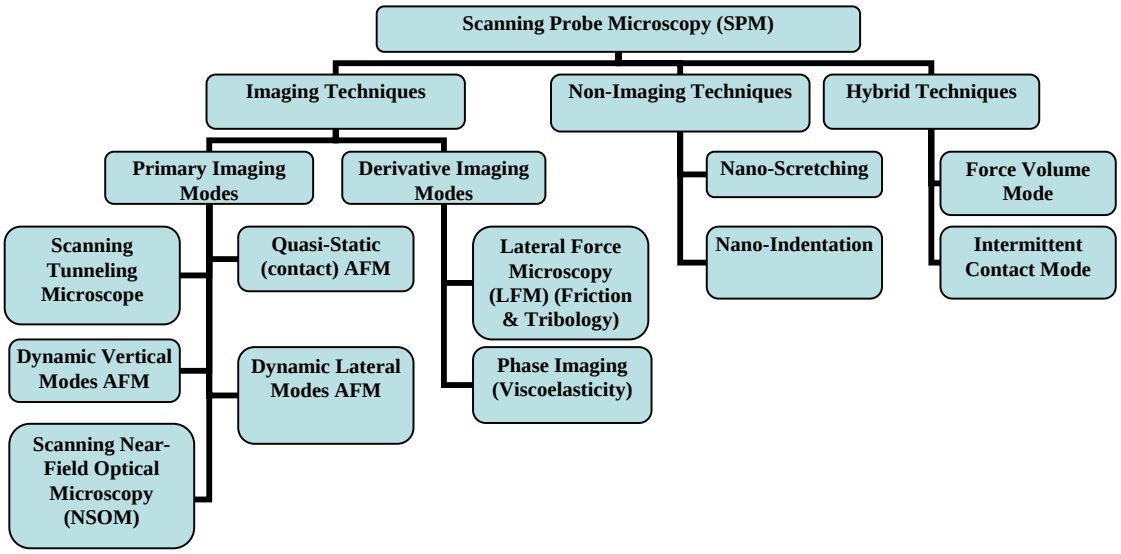

Fig.1 General Classification of Scanning Probe Microscopy (SPM)

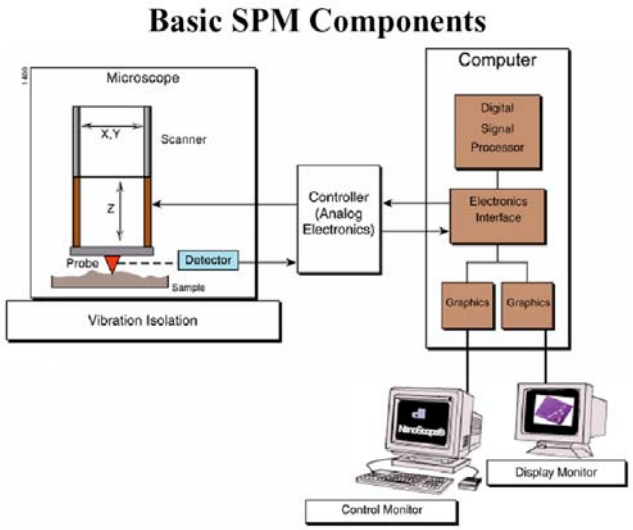

Fig. 2 MultiMode SPM Microscopy and its basics components

III. Setting Selection Optimization

For a proper use of the microscope and to get precise topography with high clarity, some parameters are controlled in the feedback mode optimization, they are: setpoint, gains, and scan speed (or scan rate). The setpoint usually governs the cantilever deflection and, consequently, determines pressure (contact) force between the tip and the surface in a way that contact force become higher as setpoint is increased.

Photodiode array with the four elements of the quad photodiode (position sensitive detector) are combined to provide different information depending on the operating mode. In all modes the four elements combine to form the SUM signal. The amplified differential signal between the top two elements and the two bottom elements provides a measure of the deflection of the cantilever. This differential signal is used directly in the contact AFM. Similarly, the amplified differential signal between the sum of two left photodiodes and the sum of the two right photodiodes provides a measure of the torsion in the cantilever and is used in Lateral Force Microscopy (Image data type: "*Friction*") [33]-[38].

IV. Experimental Setup

Five as received different types of tool inserts are tested throughout the different stages of this study; two uncoated and three multilayers coated carbide inserts. The uncoated types are Kennametal K68 and K21 carbide inserts. ISO application range for K68: M10-20 K05-20 (ANSI Range: C3). It consists of a hard, low binder content, unalloyed grade WC/Co fine-grained grade. As claimed by manufacturer, grade K68 has excellent abrasion resistance for machining cast irons, austenitic stainless steels, non-ferrous metals, nonmetals and, it is recommended by manufacturer to be used as a general purpose grade for non-ferrous materials. First tested coated carbide inserts type is Kennametal multicoated KC810 CVD coated carbide with ISO Range: P10-30 (ANSI Range: C6-C7). It consists of a multilayered coating over an alloyed carbide substrate. As recommended by manufacturer, it is used for general steel machining at low to moderate speeds. Another two types of coated carbide inserts are used in this study: Sandvik CVD multicoated GC415 and GC435. The CVD TiN-Al2O3-TiC multilayers GC415 coated inserts are intended for turning steel and cast iron (P05-30, K05-20, C6-8). As claimed by manufacturer, extremely high wear and plastic deformation of the inserts permits high metal removal rates within a broad application range. The multilayers coated

GC435 (1 μm TiN followed by 3 μm Al2O3 and finally a layer of 5 μm TiC over the sintered carbide substrate) is used for steel cutting (ISO P35 range) with decreasing rates of plastic deformation and growth of thermal and mechanical fatigue cracks. Inserts are of SPUN 12 03 12 (thickness = 3.18 mm & r=1.2 mm & l=12.7 mm, clearance angle =5-7 rake angle = 6).

V. Experimental Data, Analysis and Discussion

Nonconventional machining and metal removal techniques have used the AFM features in many applications [50], [60]-[66]. In [50], the problems of nonlinearity and low repeatability position accuracy of AFM scanner at longer scan strokes are solved using micro/nanomachining AFM system similar to conventional CNC machine tools controller. With a very light normal load on the sample surface, the AFM diamond tip is used as a cutting tool. Effects of tip geometry, the scribing direction, the normal load, the machining speed and feed on the machining depth are discussed. The influence of different machined conditions on surface characterization using AFM with limited applied load is also reported [60]-[62]. Better surface roughness is claimed to be improved with dependence on applied load, scribing cycle, scribing speed and scribing feed. Surface roughness of EDM machined surface [63] is found proportional to the power input with best values at low pulse energy. Also, it is claimed that information about depth microcracks is revealed. Laser nanomachining and nanofabrication are also frequently reported [64], [65].

NanoScope™ systems [66], digital software control of the SPM process, includes real time (i.e., all operations including preparation and manipulation of the microscope before and during scanning) manipulation of the microscope system and offline (i.e., analysis and modification of captured images) processing of captured NanoScope.

In contact AFM three data types can be simultaneously displayed; "*Height*", "*Deflection*" and "*Friction*". Height data corresponds to the change in piezo height needed to keep the cantilever deflection constant. Deflection data comes from the differential signal off of the top and bottom photodiode segments. The scan parameters required to collect good height data are different from the optimal parameters for deflection data. To collect height data, the feedback gains must be high so that the tip tracks the sample surface with minimal cantilever deflection. The position of the piezo during the scan reflects the height of the sample. Deflection data should be collected with low feedback gains so the piezo remains at a constant position relative to the sample. In this case, the tip and cantilever will be deflected by the features on the sample surface. The output fluctuations in the cantilever deflection voltage from the top and bottom photodiode segments are recorded as a measure of the variation in the sample surface. To collect accurate topographical data, the *Data type* parameter should be set to "*Height"* in most instances [66].

A wide variety of analysis functions are available in the "*Analyze"* menu in the off-line for measuring captured SPM images. The "*Roughness"* command generates a wide variety of statistics on surfaces, including classical roughness values, peak and summit texture data and surface area calculations for the entire image [13], [48], [67]-[69].

When "*Roughness"* analysis is applied to an image, the image data is automatically planefitted beforehand. This is done to accord with ASME and ISO metrological standards. Only the Raw mean parameter is exempt from this operation, being calculated from raw data only. Regarding basic roughness measurements, average roughness R_a is one of statistics used by the roughness routine are derived from ASME B46.1 ("Surface Texture: Surface Roughness, Waviness and Lay"). While Image Mean value of data contained within the image, Image Ra Arithmetic average of the absolute values of the surface height deviations measured from the mean plane.

$$R_a = \frac{1}{N}\sum_{j=1}^{N}\left|Z_j\right| \quad (1)$$

While Image Raw mean determines the mean value of image data without application of planefitting, the *Image Rmax* specifies the maximum vertical distance between the highest and lowest data points in the image.

The *Image RMS* (Rq) is the root mean square average of height deviations taken from the mean data plane, expressed as:

$$R_q = \sqrt{\frac{\sum Z_i^2}{N}} \quad (2)$$

Image *Surface area* is the three-dimensional area of the analyzed region as the sum of the area of all of the triangles formed by three adjacent data points. The *Image Area Difference%* represents the difference between the image's three-dimensional *Surface area* and its two-dimensional, footprint area. Finally, the image Z range indicates the maximum vertical distance between the highest and lowest data points in the image. (Same as Image Rmax).

VI. Experimental Results

A. Determination of the appropriate scan size

In general, the scan rate must be decreased as the scan size is increased. Scan rates of 1.5—2.5 Hz should be used for large scans on samples with tall features. High scan rates help reduce drift, but they can only be used on very flat samples with small scan sizes. In this study a scanner of type AS-12 (E) has been employed. It has a max scan size of (12×12 μm) with a vertical range up to 2.5 μm.

Three scan sizes; 2, 6 and 12 μm are independently performed in association with both "*Height"* and "*Deflection*" data type. As shown in Figs. 3-6 and summarized numerical data plotted in Figs. 7, a scan size of 12μm, especially for uncoated surfaces, generally produces a more accurate view of the surface than those captured by either 2μm or 6μm. Cutting

inserts are usually of relatively wide surface and, the bigger the scan size, the more integrated surface features and complete waviness measure to reveal [43].

B. Determination of the appropriate data type

The "*Roughness"* command generates a wide variety of statistics on surfaces. Regarding raw area Raw and mean area (Mean) for both uncoated K68 and coated KC810 carbide inserts, Fig. 8.a, the difference in the surface quality is well captured as coated surface usually has a better surface finish. However, data plotted in Fig. 8.b reveals some facts about the possible variability encountered in the measurement. This is due to the fact that the scanned area is a relatively small and it is selected randomly that may have different characteristics than other spots on the surface.

Fig. 8.d shows a comparison between uncoated K68 and coated KC810 surfaces regarding the different roughness parameters: Z range, Area difference%, Rq, Ra and Rmax.

Fig. 8.c shows the measured same parameters for both KC415 and KC435 multilayered coated surfaces. The former reveals relatively better surface finish. Figs. 8.e&f show the possible variability in the measured roughness parameters for each of KC415 and KC435 multilayered coated surfaces.

C. Data analysis using Power Spectral Density PSD

NanoScope software offers a different roughness frequency domain FFT features that is the power spectral density "*PSD*" analysis. It presents quantitative and qualitative information about the surface state extracted from scanned area image.

As shown in Fig. 9, the computed image '*PSD*" parameters include wavelength, frequency, PSD, total power, equivalent RMS (Rq in the previous section). Data can be obtained for horizontal, vertical or 2D isotropic image. Data can be displayed either for the whole captured area, for a specific marked location or for area between any specific marked domain. Additionally, "*PSD*" facilities allows for a plot of the whole scanned area.

As shown in Fig. 10.a, the total power PSD increases as scan size getting longer. A similar trend is noticed, Fig. 10.b, when RMS is intended. Good repeatability agreement is obtained when more samples are individually scanned either in *Total Power* parameter, Fig. 10.c, and *RMS*, Fig. 10.d. It is noticed that a 2D isotropic, rather than *Horizontal* or *Vertical*, analysis usually gives a relatively more meaningful topographical information of the scanned surface.

D. Section Parameter and Surface Defects

"*Section*" feature offers a useful and attractive tool to examine the surface topography and the possible existing defects [70]. Samples are sectioned to learn about their external surface profiles rather than the underside surface. The "*Section*" command displays a top view image, upon which up to three types of reference lines in any orientation and any specified length. As shown by Fig. 11, the cross-sectional profiles and Fast Fourier Transform FFT of the data along those reference lines are usually shown in separate windows. Roughness measurements are made of the surface along the defined reference line(s). Obtained surface roughness parameters includes: roughness along section line RMS and FFT spectrum along section line.

As shown by Fig. 12, the defected surface for K21 uncoated carbide is well detected in comparison to the normal surface quality within the same scanned area, Fig. 13. Defect profile has been clearly displayed with sufficient information about depth, height and roughness characteristics.

Fig. 14 shows the comparison between surface characteristics of the defected and the normal of KC810 coated carbide surface. Sectioning analysis in both horizontal and vertical direction indicates the wide variation due to surface defects. While depth range for the defected sample, Fig. 14.b, varies from -582 to 1086 nm, a corresponding range for normal surface, Fig. 14.a, is only between 77 and 221 nm. Also, RMS values are found to be 89 and 575 nm respectively.

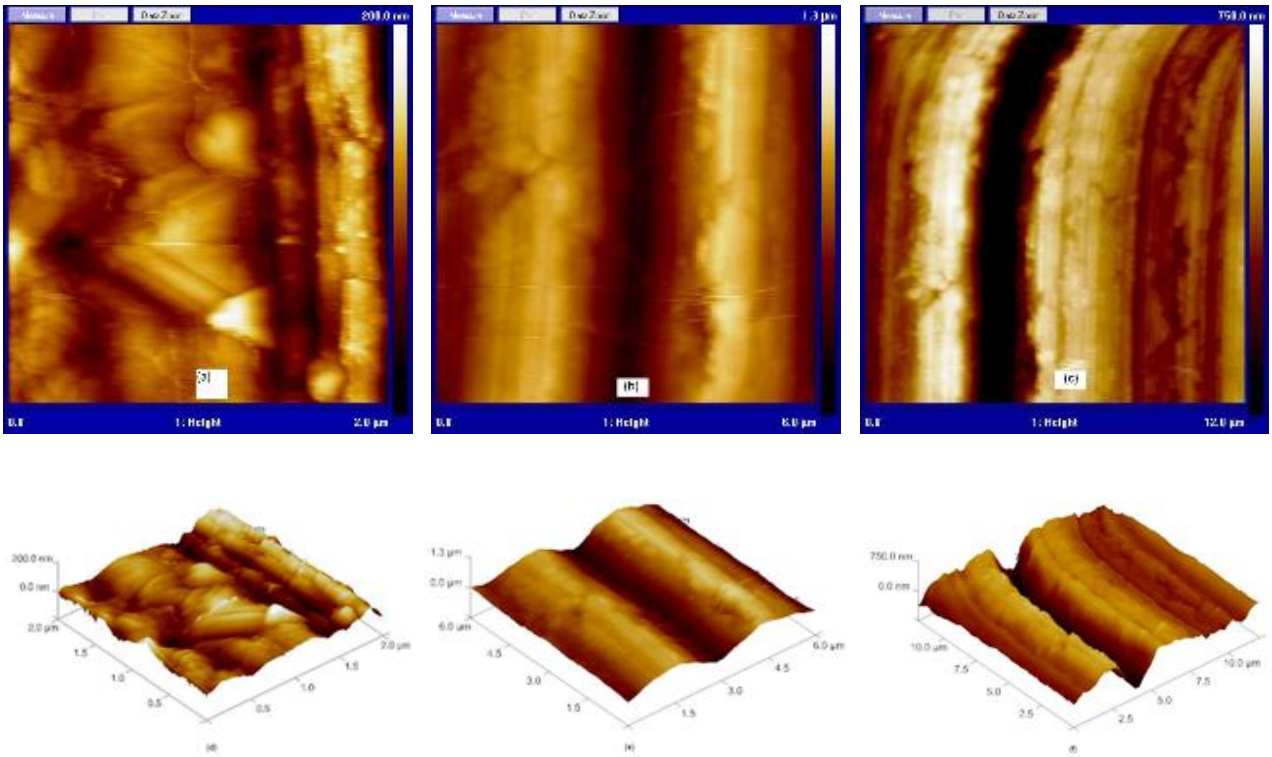

Fig. 3 Two and three dimensional "*Height*" image for different scan sizes for K68 uncoated carbide inserts

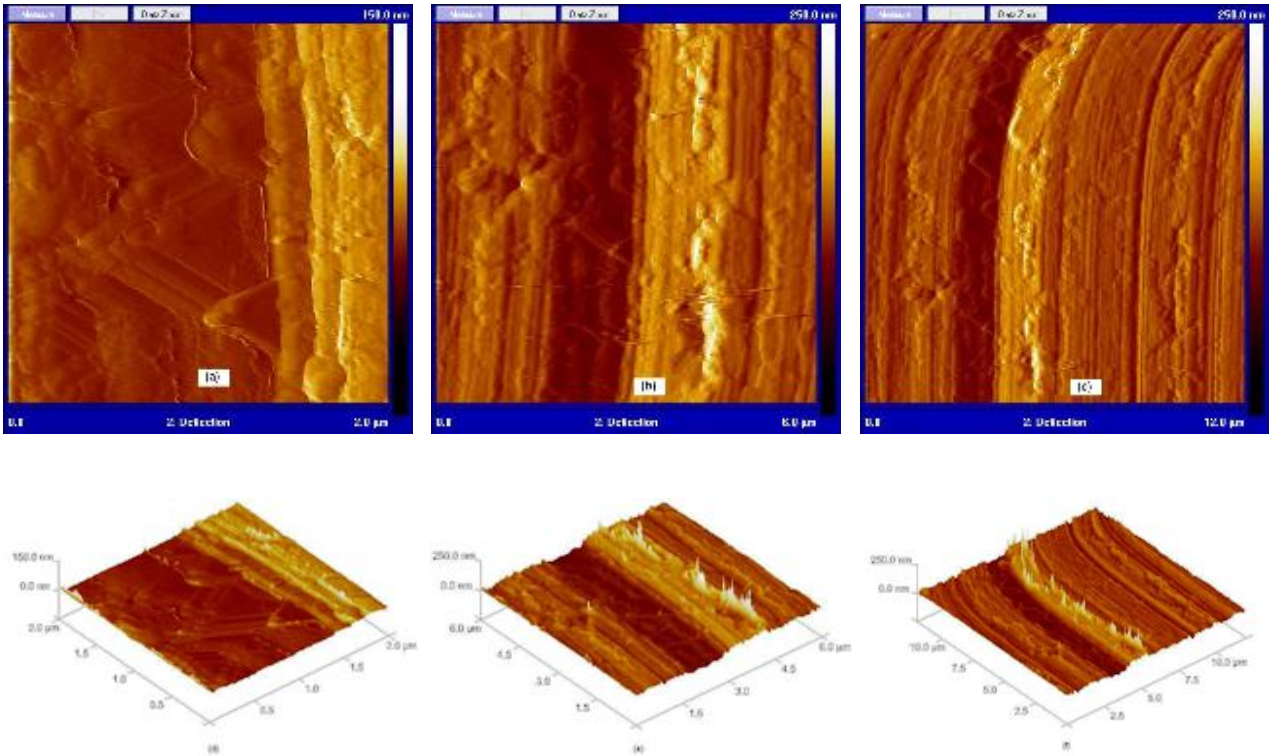

Fig. 4 Two and three dimensional "*Deflection*" image for different scan sizes for K68 uncoated carbide inserts

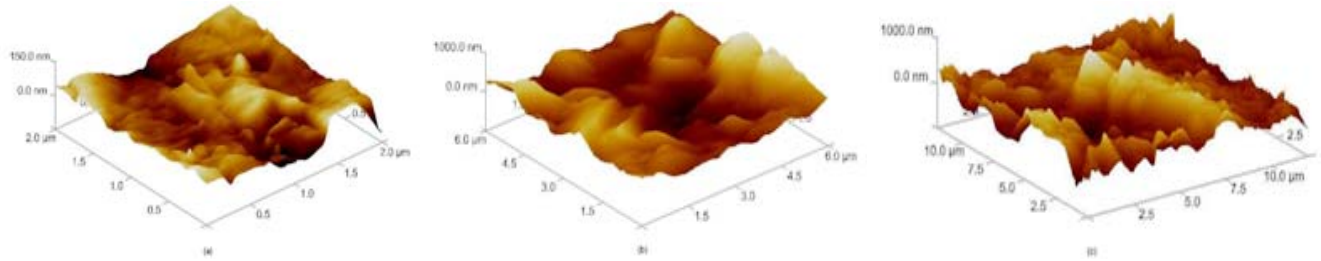

Fig. 5 Three dimensional "*Height*" image for different scan sizes for GC435 coated carbide inserts

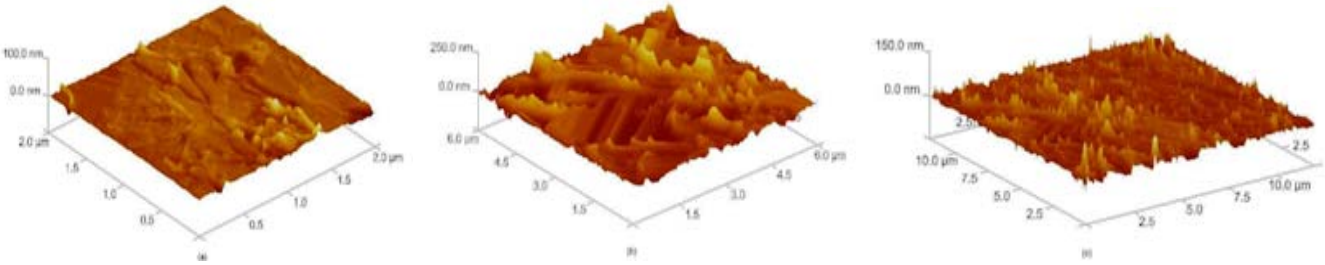

Fig. 6 Three dimensional "*Deflection*" image for different scan sizes for GC435 coated carbide inserts

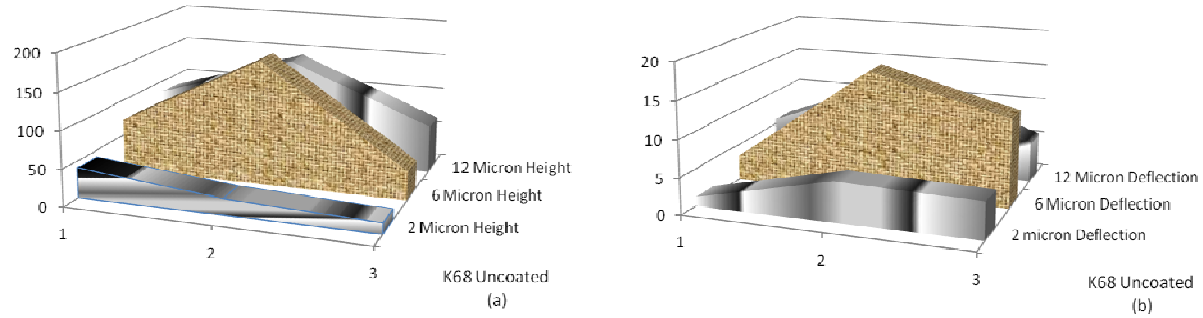

Fig. 7 Effect of scan size on "*Roughness*" Ra

VII. General Discussion

Based on the above recommended setting and manipulation of data from SPM AFM and NanoScope, a strategy is proposed here to examine surface topography and characteristics. Due to the fact that each of the data analysis modes ("*Roughness*", "*PSD*", and "*Section*") has its own special functional features, all of them are used simultaneously. The roughness analysis parameters to consider are: Zrange, surface area difference%, Rq, Ra and Rmax. Corresponding "*PSD*" parameters are: total power and equivalent RMS. However, for section analysis, the selected parameters are: spectral RMS and height range.

These interrelated and integrated nine surface controlling parameters are recommended to consider when cutting inserts surface topography is intended. Numerical data and values of the recommended controlling parameters are listed in Tables I, for K68 uncoated carbide inserts and, in table II for KC415 multilayer coated carbide inserts. As concluded in the aforementioned section, data are extracted from "*Height*" data type image analysis using a 12 μm scan size. As shown in Tables I and II, data is arranged in three distinctive groups: "*Section*", "*Roughness*", and "*PSD*". In section group, the height (depth) range indicates the difference between max and min height at the marked location while RMS gives indication about the fluctuation and profile of the intended line. Measured "*PSD*" parameters for are also included in tables as total power and equivalent RMS. While the former is an indication of surface roughness, or sum of spectral amplitudes of the surface waviness, the latter is the root mean squares around the reference mean plane for the entire intended area.

As listed in Table 1, the measured parameters for different scanned samples give sufficient information and clear idea, on one hand, about the features of the specimen surface and, on the other hand, produce a definite base for comparison among the different samples surfaces. All parameters for sample 4 reveal higher values in comparison to the first three samples due to specimen surface defect. Parameters reveal higher values for samples 1 and 2 than for sample 3. This is due to some localized defect. These values are drastically increased for sample 4 as surface is getting more rough than usual.

Table II lists measured parameter for unused, samples 1-4, and worn, samples 5-8 KC415 multilayers coated carbide inserts. Samples 3 and 4 represent specimen with normal

surfaces while the rest of samples are differently affected by various surface deterioration reasons. Sample 1 reveals a surface pinhole defect while sample 2 shows some coating droplets. Samples 5-8 show the effect of wear on different positions of tool face (rake face or crater).

A SEM micrograph of the specimen and the scanned positions are shown in Fig. 15.

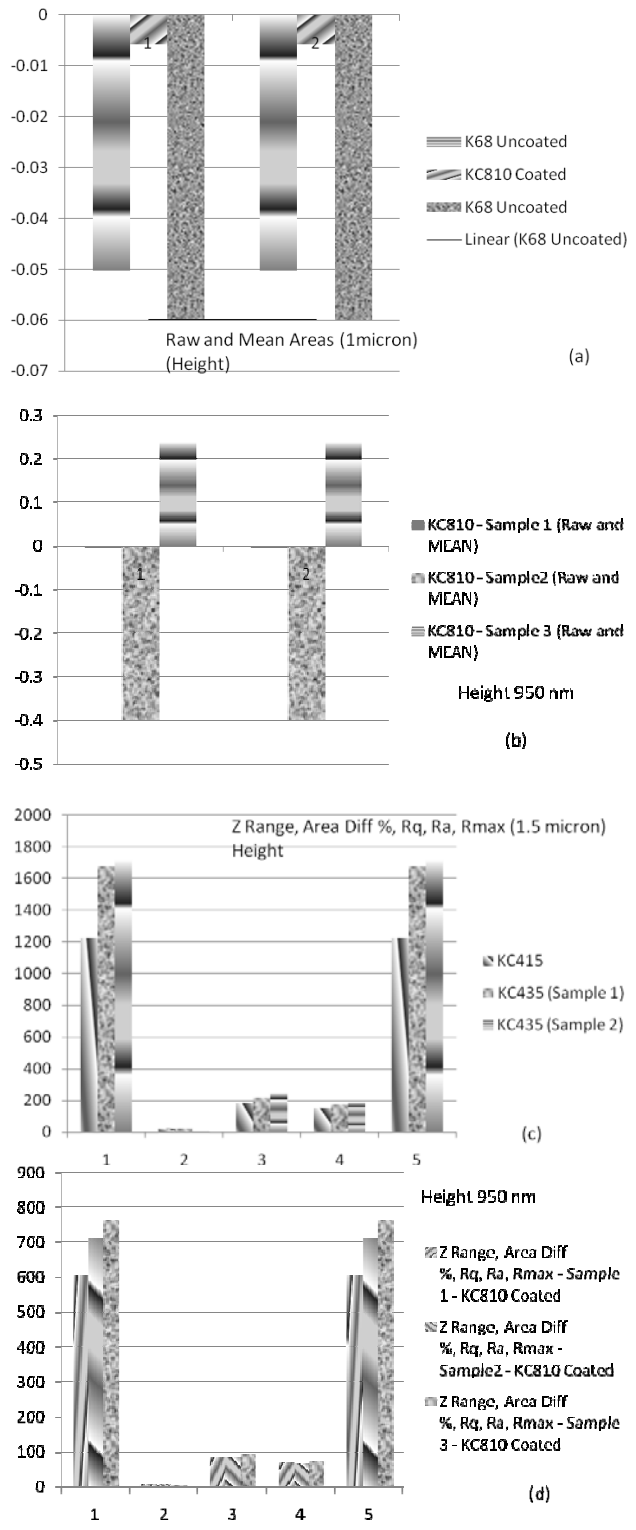

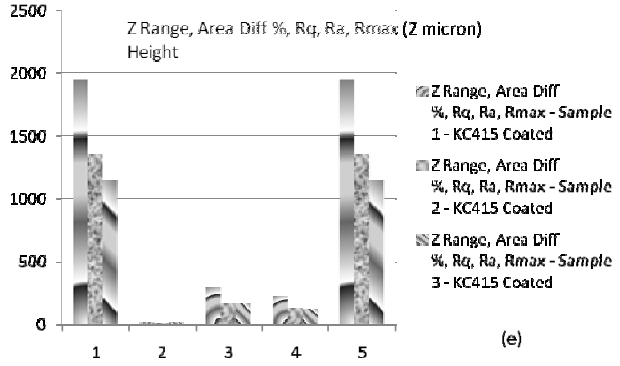

Fig. 8 Surface roughness characteristics of coated and uncoated carbides using "*Height*" data type

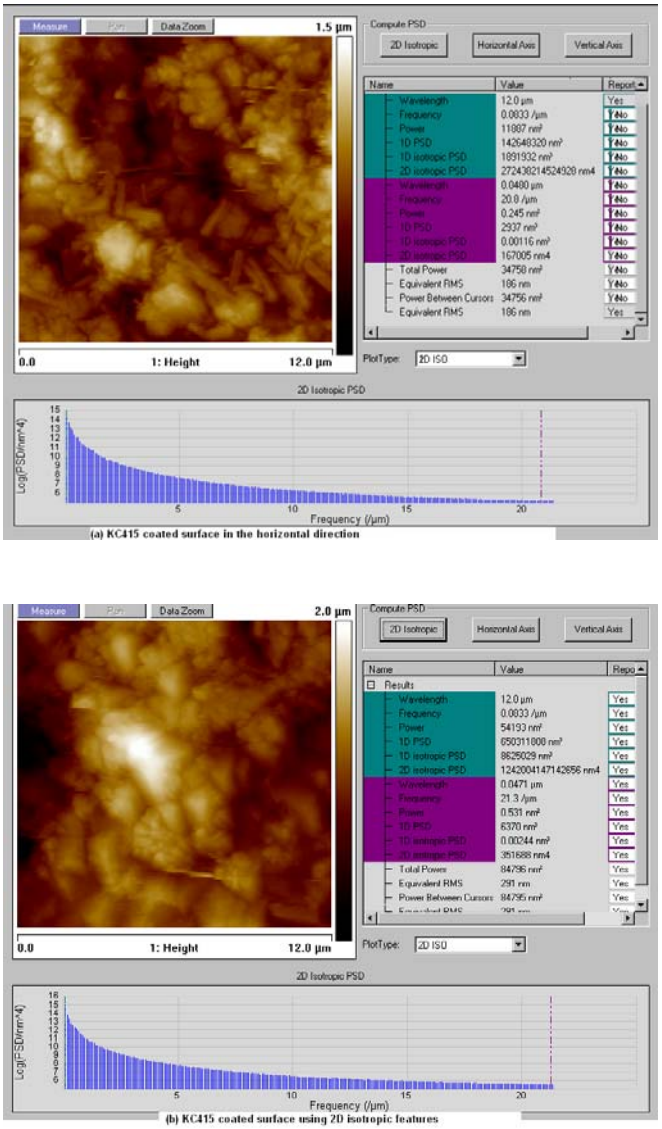

Fig. 9 Single and 2D isotropic "*PSD*" features

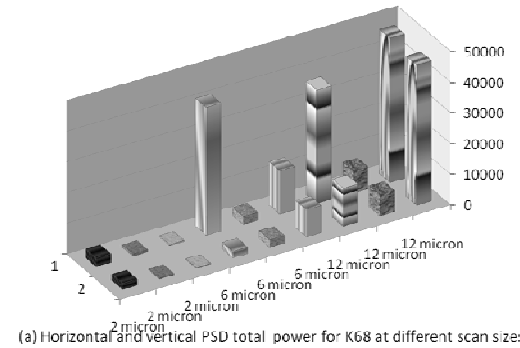

(a) Horizontal and vertical PSD total power for K68 at different scan sizes

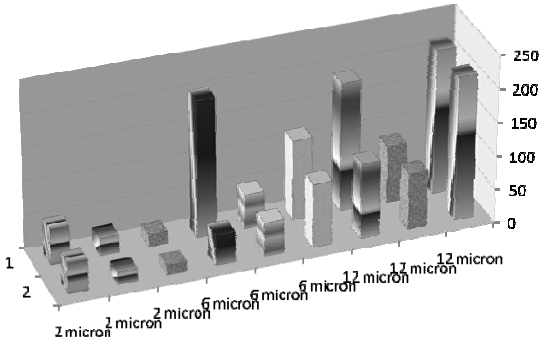

(b) Horizontal vs vertical PSD RMS for K68 at different scan sizes

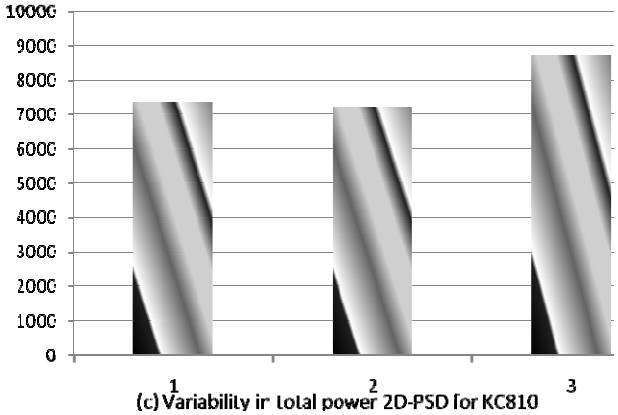

(c) Variability in total power 2D-PSD for KC810

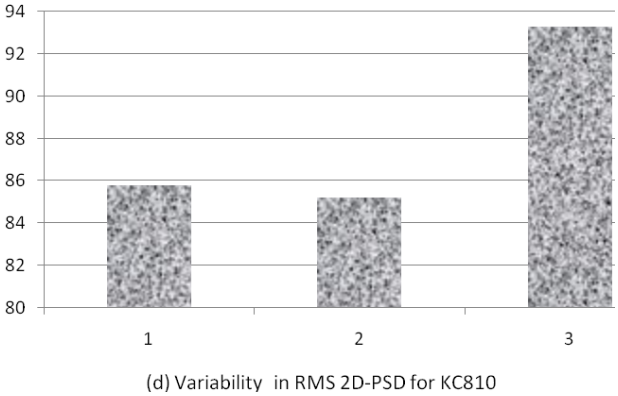

(d) Variability in RMS 2D-PSD for KC810

Fig. 10 Various parameters involved in "*PSD*" analysis

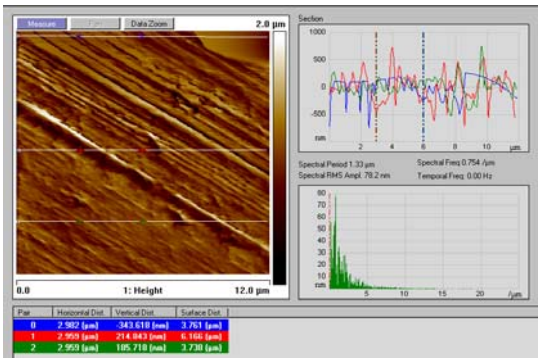

Fig. 11 "*Section*" for surface defect of K68 uncoated carbide insert

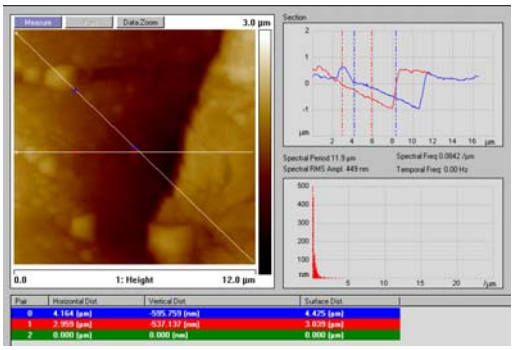

Fig. 12 "*Section*" for surface defect of K21 uncoated carbide inserts

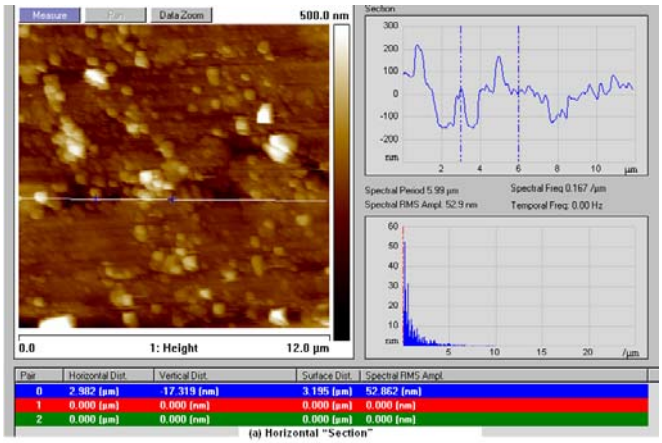

(a) Horizontal "Section"

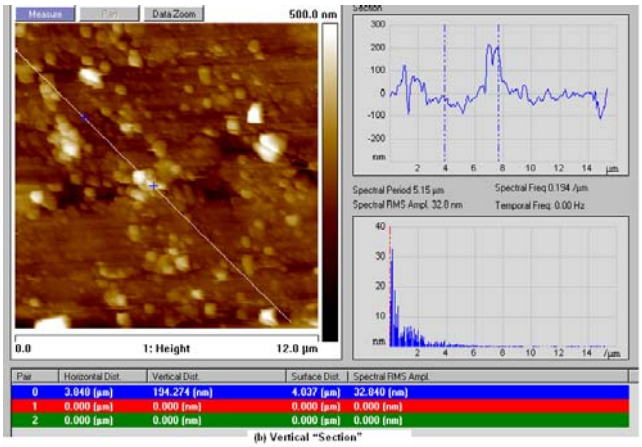

(b) Vertical "Section"

Fig. 13 "*Section*" for normal surface of K21 uncoated carbide

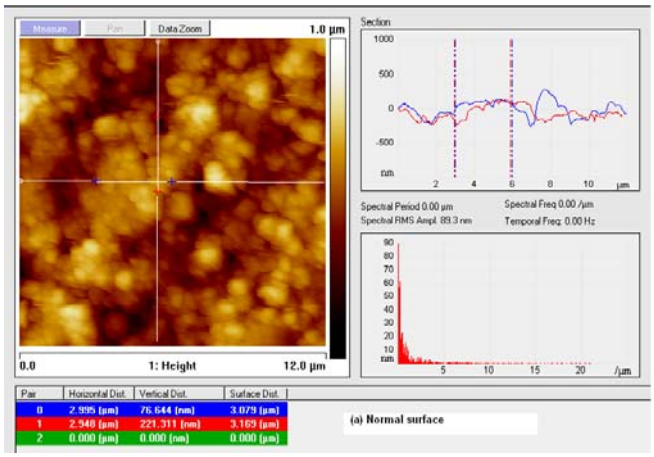

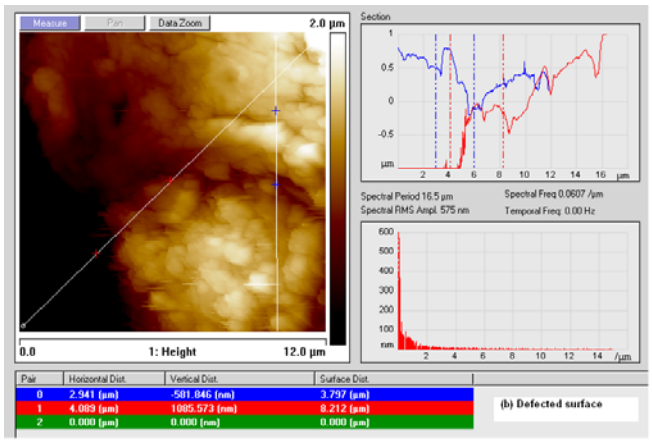

Fig. 14 "*Section*" analysis for surface examination of KC810 multilayered coated carbide inserts

TABLE I
RECOMMENDED SURFACE CONTROLLING PARAMETERS FOR K68 UNCOATED CARBIDE

Samp. No	Z level (nm)	Section Data: RMS (nm)	Section Data: Height Range (nm)	Roughness data: Area Diff. %	Roughness data: Rq (nm)	Roughness data: Ra (nm)	Roughness data: Rmax (nm)	PSD Data: Total Power (nm^2)	PSD Data: Equiv. RMS (nm)	3D Image
	1000	146	-250 To 600	36.1	119	83.9	1281	8882	94.2	
	1000	122	-500 To 310	11.1	192	144	1114	12400	111	
3	1000	101	-300 To 200	9.24	84.3	65.8	634	6858	82.9	
4	2000	782	-750 To 750	222	217	161	2855	45703	214	

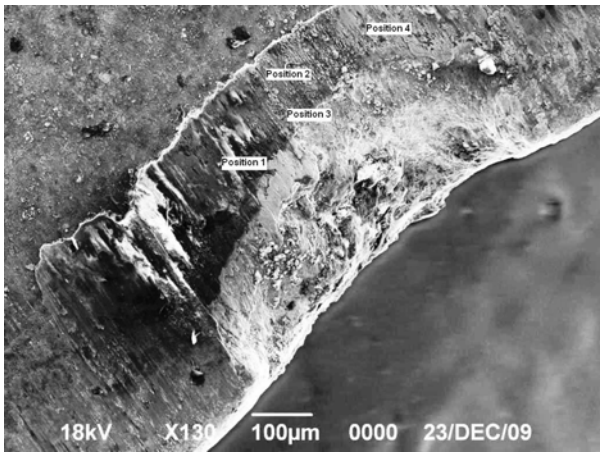

Fig. 15 Notch wear SEM micrograph of KC415 coated inserts

TABLE II
RECOMMENDED SURFACE CONTROLLING PARAMETERS FOR KC415 MULTILAYERS COATED CARBIDE

Samp. No	Z level (nm)	Section Data: RMS (nm)	Section Data: Height Range (nm)	Roughness data: Area Diff. %	Roughness data: Rq (nm)	Roughness data: Ra (nm)	Roughness data: Rmax (nm)	PSD Data: Total Power (nm^2)	PSD Data: Equiv. RMS (nm)	3D Image
1	1500	208	-500 To 485	22.3	186	112	1224	34758	186	
2	2000	432	±1000	21.4	291	227	1954	84796	291	
3	2000	86.7	-350 To 390	12.4	168	130	1356	28267	168	
4	2000	146	-450 To 490	18.3	164	128	1148	26913	164	
5	500	78.9	-160 To 200	5.84	90.2	73.4	612	8143	90.2	
6	6000	818	-800 To 2000	107	500	398	2866	530032	728	
7	6000	815	0 To 2000	31.1	311	236	2204	123790	352	
8	2000	160	±250	8.09	123	97.4	839	43666	209	

VIII. FRICTION SURFACE TOPOGRAPHY OF COATED AND UNCOATED CARBIDE INSERTS

One of the most useful AFM modes in friction and tribological applications is the lateral force microscopy. In the employed MultiMode SPM, lateral force mode can be activated as a derivative to the main contact mode. Therefore, in addition to "*Height*" and "*Deflection*" images, a third one is obtained: "*Friction*".

As "*Height*" and "*Deflection*" data provides information about the surface topography along the axis, "*Friction*" data determines the cantilever tilting perpendicular to the scanned

axis. This is caused by both friction and the tip running into or tripping on the edges of features that yields a map of high- and low-friction sites. Signals for "*Friction*" data types are the output of the amplified differential signal between the sum of two left photodiodes and the sum of the two right photodiodes.

Generally, Friction data type gives valuable information about surface topography normal to scanning direction. Friction image and its analysis have been extensively used in many researches and application fields [7], [9], [10], [13], [14], [19], [39]-[44]. In the current study, however, an explanation is given of how friction analysis can be used as a useful indicator of the surface topography of tool inserts.

In order to get relative information considering friction parameter, the area difference % in roughness analysis is used as a criterion judgement. Area difference % shows the difference between the scanned and the projected areas which gives a meaningful physical indication about surface quality. One advantage of using such a parameter resides in it is a dimensionless measure which allows the absolute comparison between the studied three data types: "*Height*" , "*Friction*" and "*Deflection*". However, it should be emphasized here that "*Height*" data usually offers information about the surface roughness produced by asperities in the scanned direction while "*Friction*" data generates data regarding the pattern and distribution of these asperities.

Fig. 16 shows the measured friction values in comparison to height and deflection counterparts for both k68 uncoated and KC810 multilayers coated carbide inserts at different scan sizes; 2, 6 and 12 μm. As shown in the figure, there is an additional proof that a 12 μm scan size is the preferred size to use regarding the specific purpose of the current study.

Fig. 17 shows a comparison between height and friction imaging data types considering sample 2 of K68 uncoated carbide inserts, Table I. The existing surface groove, Fig. 17.a, is detected by "Friction" image, Fig. 17.b, as positive values revealing that the probe tip has practiced high twisting, tilting or torque when going down the groove. Friction data type using area difference %, is found 98 times larger the corresponding value from height data type.

Also, Fig. 17 shows a comparison between height and friction imaging data types considering sample 8 of KC810 multilayer coated carbide, Table II. A coating droplet with irregular configuration is found to ruin surface quality both in the scanned and the lateral (friction) directions revealing. Roughness pattern in the lateral direction is found 79 times higher than that measured by height data analysis.

In conclusion, the use of "*Height*" data in association with the counterpart "*Friction*" data gives a promising quantitative and qualitative assessment of the topography and defects experienced on the insert surface: coating droplets, microcracks, surface grinding and preparation, etc. While height data produces an absolute judgment about the extent of surface roughness over the entire area in the scanned direction, friction data introduces an attractive indication about the roughness pattern in the lateral direction. To avoid the possible variation in output unit and scale, area difference% offers a good comparative criterion parameter to use.

Nevertheless, it should be argued here that more analysis is still required to elucidate some technical relevant topics. Among theses topics are: whether an identical outcome will be obtained when procedures are repeated with exchanging direction and, whether a universal definitive measured criterion is evaluated for height-friction mutual correlation, or interrelation considering wider ranges of tested materials and scanned sizes. This is the main object of a study under processing by researchers involved in the current research.

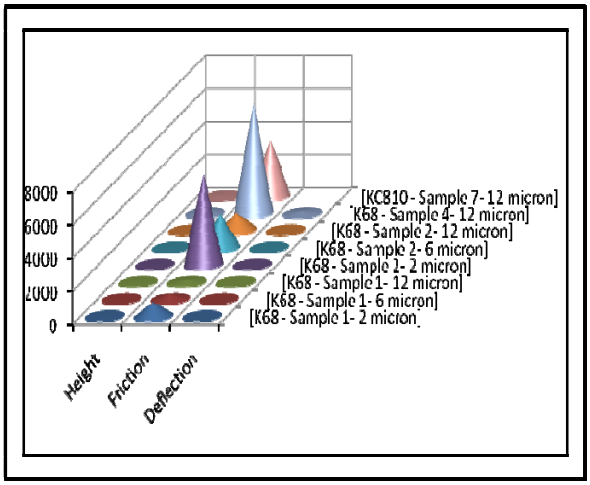

Fig. 16 Comparison between "*Height*", "*Deflection*" and "*Friction*" for defects-free and defected coated and uncoated carbide inserts

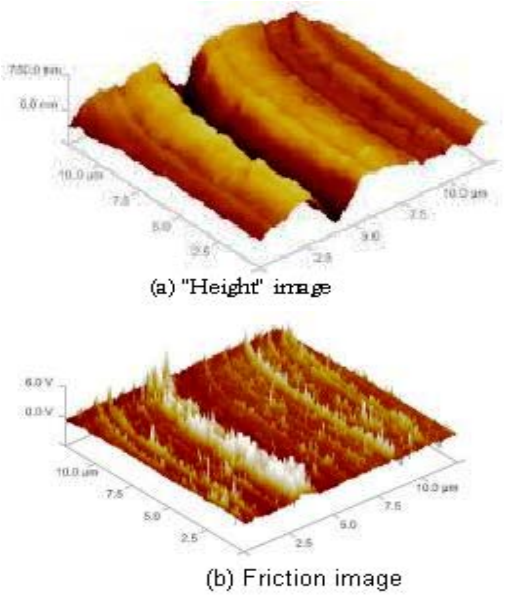

Fig. 17 "*Height*" and "*Friction*" for K68 uncoated carbide inserts

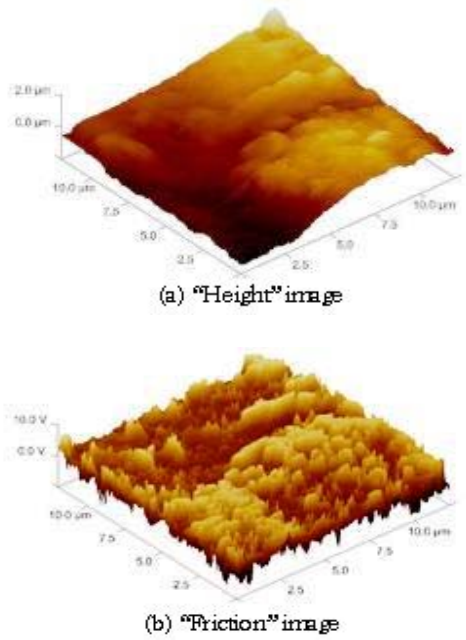

Fig. 18 "*Height*" and "*Friction*" for KC810 coated carbide inserts

IX. Conclusion

In this study, it is shown how the AFM contact mode features may be used to characterize the surface topography of the coated and uncoated cutting tools carbide inserts. Prior examination of the cutting insert is important to assess its prospective performance when utilized in real machining. Among three employed scan sizes, it is found that larger scanned area generally produces more precise assessment of the intended surface topography. "*Height*" imaging data type is found to be more representative measure than its counterpart derivative "*Deflection*". While "*Roughness*" parameter, with various statistical measures, produces information about both absolute and comparative levels of surface topography, "*PSD*" provides FFT statistical features of the scanned surface. Surface defects, including microcracks, coating pinhole and droplet have been well detected and evaluated using "*Section*" parameter. It is shown that the "*Friction*" data type, as a lateral (perpendicular) signal to "*Height*", is very useful to examine the surface topography through the difference percent between the actual and the projected scanned area. Many manufacturing, preparation and conventional surface defects are visualized through the promising still to require more investigation "*Friction*" analysis.

Acknowledgment

Authors wish to thank the Public Authority for Applied Education and Training PAAET, KUWAIT State for supporting the current project (TS-09-09). Also, thank is extended to the director, technical and administrative staff of EUN, Faculty of Science, Kuwait University for their unlimited help and cooperation during the use of their Lab facilities especially AFM and SEM.

References

[1] G. Binnig and C. F. Quate, "Atomic Force Microscope," *Physical Review Letters,* vol. 9, no. 9, pp. 930-933, 1986.
[2] M. Nakamura and H. Tokumoto, "Molecular arrangement of copper phthalocyanine on Si(001)-(2 x 1)-H: a high-resolution frictional force microscopy and molecular mechanics study," *Surface Science,* vol. 398, no. 1, pp. 143-153, Feb. 1998.
[3] T. Gray, J. Killgore, J. Luo, A. Jen and R. Overney, "Molecular mobility and transitions in complex organic systems studied by shear force microscopy," *Nanotechnology,* vol. 18, pp. 1-9, 2007.
[4] A. Noy *et al.*, "Chemically-Sensitive imaging in tapping mode by chemical force microscopy: Relationship between phase lag and adhesion," *Langmuir,* vol. 14, no. 7, pp. 1508-1511, 1998.
[5] R. Maoz, S. Cohen and J. Sagiv, "Nanoelectrochemical patterning of monolayer surfaces: Toward spatially defined self-assembly of nanostructures," *Advanced Materials,* vol. 11, no. 1, pp. 55–61, 1999.
[6] A. Ebner *et al.*, "Recognition imaging using atomic force microscopy," *in Handbook of Single-Molecule Biophysics,* Springer Science+Buisiness Media, 2009, ch. 18, pp. 524-551.
[7] J. Houston *et al.*, "Comparative study of the adhesion, friction, and mechanical properties of CF3- and CH3-terminated alkanethiol monolayers," *Langmuir,* vol. 21, no. 9, pp. 3926-3932, 2005.
[8] R. Carpick, D. Sasaki and A. Burns, "Large friction anisotropy of a polydiacetylene monolayer," *Tribology Letters,* vol. 7, no. 2-3, pp. 79–85, 1999.
[9] H. Schumacher *et al.*, "Controlled mechanical AFM machining of two-dimensional electron systems: fabrication of a single-electron transistor," *Physica,* vol. 6, no. 1-4, pp. 860-863, Feb. 2000.
[10] M. Enachescu *et al* "Atomic force microscopy study of an ideally hard contact: The diamond (111)/ tungsten carbide interface," *Physical Review Letters,* vol. 81, no. 9, pp. 1877-1880, 1998.
[11] B. Bhushan, J. Israelachviii and U. Landman, "Nanotribology, friction, wear and lubricant at atomic scale," *Nature,* vol. 374, pp. 607-616, 1995.
[12] B. Sumer and M. Sitti, "Rolling and Spinning Friction Characterization of fine particles using lateral force microscopy based contact pushing," *J. Adhesion Science Technology,* vol. 22, pp. 481-506, 2008.
[13] X. Peng, Z. Barber and T. Clyne, "Surface roughness of diamond-like carbon films prepared using various techniques," *Surface and Coatings Technology,* vol. 138, pp. 23-32, 2001.
[14] B. Bhushan, "Nanotribology and nanomechanics," *Wear*, vol. 259, pp. 1507–1531, 2005.
[15] N. Tambe and B. Bhushan, "Scale dependence of micro/nano-friction and adhesion of MEMS/NEMS materials, coatings and lubricants," *Nanotechnology*, vol. 15, no. 11, pp. 1561-1570, 2004.
[16] S. Kopta and M. Salmeron, "The atomic scale origin of wear on mica and its contribution to friction," *J. Chemical Physics,* vol. 113, no. 18, pp. 8249-8252, 2000.
[17] G. Garcia-Ayuso, L. Vázquez and J. Martínez-Duarta, "Atomic force microscopy (AFM) morphological surface characterization of transparent gas barrier coatings on plastic films," *Surface and Coatings Technology*, vol. 80, no. 1-2, pp. 203-206, 1996.
[18] M. Sato *et al.*, "Local mechanical properties measured by atomic force microscopy for cultured bovine endothelial cells exposed to shear stress,". *J. Biomechanics*, 2000, 33 (1), 127-135.
[19] J. Li *et al.*, "Friction coefficients derived from apparent height variations in contact mode atomic force microscopy images," *Langmuir*, vol. 15, no. 22, pp. 7662-7669, 1999.
[20] K. Cheng, X. Luo and R. Holt, "Modelling and simulation on the tool wear in nanometric cutting," *Wear*, vol. 255, no. 7, pp. 1427-1432, 2003.
[21] K. Komai, K. Minoshima S. and Inoue, "Fracture and fatigue behavior of single crystal silicon microelements and nanoscopic AFM damage evaluation," *Microsystem Technologies*, vol. 5, no. 1, pp. 30-37, 1998.
[22] http://nano.tm.agilent.com.
[23] M. Falvo *et al.*, "Manipulation of individual viruses: Friction and mechanical properties," *Biophysical Journal*, vol. 72, pp. 1396-1403, 1997.
[24] T. Chung, D. Liu, S. Wang and S. Wang, "Enhancement of the growth of human endothelial cells by surface roughness at nanometer scale," *Biomaterials*, vol. 24, pp. 4655-4661, 2003.
[25] C. Grimellec *et al.*, "Imaging of the surface of living cells by low-force contact-mode atomic force microscopy," *Biophysical Journal*, vol. 75, pp. 695-703, 1998.

[26] K. Barbee, P. Davies and R. Lal, "Shear stress-induced reorganization of the surface topography of living endothelial cells imaged by atomic force microscopy," *Circulation Research, American Heart Association (http://circres.ahajournals.org)*, vol. 74, pp. 163-171, 1994.

[27] B. Rodriguez *et al.*, "Electromechanical imaging of biomaterials by scanning probe microscopy," *Journal of Structural Biology*, vol. 153, pp. 151-159, 2006.

[28] M. Yan *et al.*, "On the ductile machining of silicon for micro electro-mechanical systems (MEMS), opto-electronic and optical applications," *Materials Science and Engineering*, A29, pp. 230-234, 2001.

[29] Application notes of ASYLUM RESEARCH (www.AsylumResearch.com).

[30] AFM Resource Library – Agilnet Technology (www.afmuniversity.org).

[31] C. Schmitt, J. Elings and M. Serry, "Nanoindenting, Scratching, and wear testing with the atomic force microscope, solutions for a nanoscale world," *Veeco Instruments Inc*., (www.veeco.com).

[32] F. Peter, A. Rüdiger and R. Waser, "Mechanical crosstalk between vertical and lateral piezoresponse force microscopy," *Review of scientific instruments*, vol. 77, 036103, pp. 1-3, 2006.

[33] A. Hoffmann, T. Jungk and E. Soergel, "Crosstalk correction in atomic force microscopy," *Review of scientific instruments,* vol. 78, no. 1, 2007, 016101, doi:10.1063/1.2424448.

[34] P. Prunici and P. Hess "Quantitative characterization of crosstalk effects for friction force microscopy with scan-by-probe SPMs," *Ultramicroscopy*, vol. 108, pp. 642-645, 2008.

[35] M. Varenberg, I. Etsion and G. Halperin, "Crosstalk problems in scanning-by-probe atomic force microscopy," *Review of scientific instruments*, vol. 74, no. 7, pp. 3569-3571, 2003.

[36] D. Richard, R. Piner, S. Rodney and R. Ruoff, "Cross talk between friction and height signals in atomic force microscopy," *Review of scientific instruments*, vol. 73, no. 9, pp. 3392-3394, 2002.

[37] G. Michal, C. Lu and A. Tieu, "Influence of force-based crosstalk on the 'wedge method' in lateral force microscopy," *Measurement Science Technology*, vol. 20, 2009, doi: 10.1088/0957-0233/20/5/055103.

[38] C. Onal, B. Sümer and M. Sitti, "Cross-talk compensation in atomic force microscopy," *Review of scientific instruments*, vol. 79, no. 10, 2008, 103706, doi:10.1063/1.3002483.

[39] R. Piner, D. Richard, R. Ruoff and S. Rodney, "Effect of friction on height measurement of < 1nm via AFM," *American Physical Society,* in the Annual APS Meeting, Indiana Convention Center, Indianapolis, Indiana Meeting, March 18-22, 2002.

[40] S. Sundararajan and B. Bhushan, "Topography-induced contributions to friction forces measured using an atomic force/friction force microscope," *J. Applied Physics*, vol. 88, 4825, 2000, 4825, doi:10.1063/1.1310187.

[41] A. Yurtsever, A. Gigler and R. Stark, "Amplitude and frequency modulation torsional resonance mode atomic force microscopy of a mineral surface," *Ultramicroscopy*, vol. 109, no. 3, pp. 275-279, 2009.

[42] S. Park, K. Costa and G. Ateshian, "Microscale frictional response of bovine articular cartilage from atomic force microscopy," *J Biomechanics*, vol. 37, no. 11, pp. 1679-1687, 2004.

[43] V. Koinkar and B. Bhushan, "Effect of scan size and surface roughness on microscale friction measurements," *J. Applied. Physics*, vol. 81, 2472, 1997, doi:10.1063/1.363954.

[44] A. Shegaonkar, C. Lee and S. Salapaka, "Feedback scheme for improved lateral force measurement in atomic force microscopy," in *2008 American Control Conference,* Westin Seattle Hotel, Seattle, Washington, USA, June 11-13, 2008.

[45] C. Baur *et al.*, "Nanoparticle manipulation by mechanical pushing: underlying phenomena and real-time monitoring," *Nanotechnology*, vol. 9, pp. 360-364, 1998.

[46] S. Youn *et al.*, "AFM, SEM and nano/micro-indentation studies of the fib-milled glassy carbon surface hat-treated at different conditions," *MEMS and Packaging Group, Advanced Manufacturing Research Institute, National Institute of Advanced Industrial Science and Technology (AIST),* Stresa, Italy, 26-28 April 2006.

[47] Nanoindentation and Nanoscratching with SPMs for NanoScope™ Version 4.32 Software. Support Note No. 225, Rev. F, Digital Instruments, 1998, 112 Robin Hill Road, Santa Barbara, CA 93117.

[48] B. Bhushan and T. Kasai, "A surface topography-independent friction measurement technique using torsional resonance mode in an AFM," *Nanotechnology*, vol. 15, 923, 2004, doi: 10.1088/0957-4484/15/8/009.

[49] M. Bische, M. Vanlandingham, R. Eduljee, Jr. Gillespie and J. Schultz, "On the use of nanoscale indentation with the AFM in the identification of phases in blends of linear low density polyethylene and high density polyethylene," *Journal of Materials Science*, vol. 35, no. 1, pp. 221-228, 2000.

[50] Y. Yan, T. Sun, Y. Liang and S. Dong, "Investigation on AFM-based micro/nano-CNC machining system," *International Journal of Machine Tools & Manufacture*, vol. 47, pp. 1651-1859, 2007.

[51] G. Schitter, G. Fantner, J. Kindt, P. Thurner and P. Hansma, "On recent developments for high-speed atomic force microscopy," in *Proc. of the IEEE/ASME, International Conference on Advanced Intelligent Mechatronics, Monterey,* California, USA, July 24-28, 2005, pp. 261-264.

[52] P. Vettiger *et al.*, "The "Millipede" nanotechnology entering data storage," *IEEE/ASME Trans on Nanotechnology*, vol. 1, no. 1, pp. 39-55, 2002.

[53] R. Carpick, N. Agraýt, D. Ogletree and M. Salmeron, "Variation of the interfacial shear strength and adhesion of a nanometer-sized contact," *Langmuir*, vol. 12, pp. 3334-3340, 1996.

[54] T. Larsen and K. Molonia, "Comparison of wear characteristics of etched-silicon and carbon nanotube atomic-force microscopy probes," *Applied Physics letters*, vol. 80, no. 11, pp. 1996-1998, 2002.

[55] G. Li, N. Xi, M. Yu and W. Fung, "Development of augmented reality system for AFM-based nanomanipulation,". *IEEE/ASME Trans on Mechatronics*, vol. 9, no. 2, pp. 358-365, 2004.

[56] S. Kalinin *et al.*, "Vector piezoresponse force microscopy," *Microscopy and Microanalysis, Microscopy Society of America*, vol. 12, pp. 206-220, 2006.

[57] M. Varenberg, I. Etsion and G. Halperin, "An improved wedge calibration method for lateral force in atomic force microscopy," *Review of Scientific Instruments*, vol. 74, no. 7, pp. 3362-3367, 2003.

[58] M. Bloo, H. Haitjem and W. Pril, "Deformation and wear of pyramidal, silicon-nitride AFM tips scanning micrometre-size features in contact mode measurement," *Measurement*, vol. 25, no. 3, pp. 203-211, 1999.

[59] MultiMode™ SPM Instruction Manual Version 4.31ce, 1996-99 Digital Instruments, Veeco Metrology Group.

[60] T. Jung *et al.*, "Atomic force microscope used as a powerful tool for machining surfaces," *Ultramicroscopy*, vol. 42-44 (B), pp. 1446-1451, 1992.

[61] T. Fang and W. Chang, "Effects of AFM-based nanomachining process on aluminum surface," *Journal of Physics and Chemistry of Solids*, vol. 64, pp. 913-918, 2003.

[62] T. Fang, C. Weng and J. Chang, "Machining characterization of the nano-lithography process using atomic force microscopy," *Nanotechnology*, vol. 11, pp. 181-187, 2000.

[63] Y. Guu, "AFM surface imaging of AISI D2 tool steel machined by the EDM process," *Applied Surface Science*, vol. 242, pp. 245-250, 2005.

[64] J. Cheng, C. Wei, K. Hsua and T. Toung, "Direct-write laser micromachining and universal surface modification of PMMA for device development," *Sensors and Actuators, B*, vol. 99, pp. 186-196, 2004.

[65] A. Chimmalgi, T. Choi, C. Grigoropoulos and K. Komvopoulos, "Femtosecond laser aperturless near-field nanomachining of metals assisted by scanning probe microscopy," *Applied Physics Letters*, vol. 82, no. 8, pp. 1146-1148, 2003.

[66] NanoScope Software 6.13 User Guide. 2004, Veeco Instruments Inc.

[67] C. Poon and B. Bhushan, "Comparison of surface roughness measurements by stylus profiler, AFM and non-contact optical profiler," *Wear*, vol. 190, pp. 76-88, 1995.

[68] S. Sundararajan and B. Bhushan, "Static friction and surface roughness studies of surface micromachined electrostatic micromotors using an atomic force/friction force microscope," *J. Vacuum Science Technology*, vol. 19, no. 4, pp. 1777-1785, 2001.

[69] G. Simpson, D. Sedin and K. Rowlen, "Surface roughness by contact versus tapping mode atomic force microscopy," *Langmuir*, vol. 15, no. 4, pp. 1429-1434, 1999.

[70] A. Ankudinov *et al.*, "Cross-sectional atomic force microscopy of ZnMgSSeand BeMgZnSe-based laser diodes," *Applied Physics Letters*, vol. 75, no. 17, pp. 2626-2629, 1999.